Supplementary material:

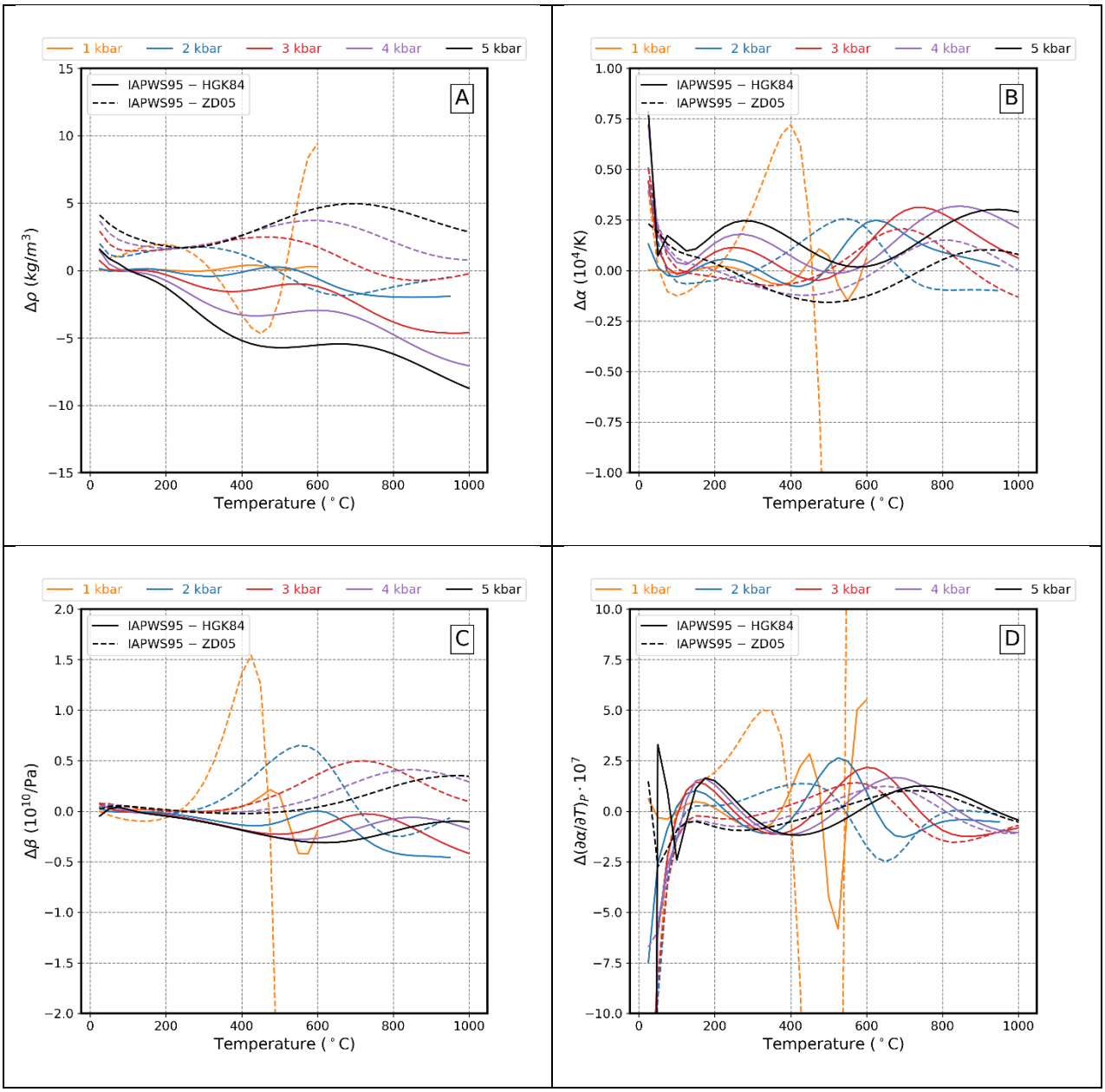

Figure S1. Plots showing the differences in the volumetric properties of water calculated using the HGK84 and ZD05 formulations from those obtained using the IAPWS95 model (25-1000 °C, 1-5 kbar): (A) ρ_{H_2O} (water density), (B) $\alpha_{\mathrm{H_2O}}$ (isobaric expansivity), (C) $\beta_{\mathrm{H_2O}}$ (isothermal compressibility), (D) $(\partial\alpha/\partial T)_P$ (isobaric temperature derivative of the isobaric expansivity).

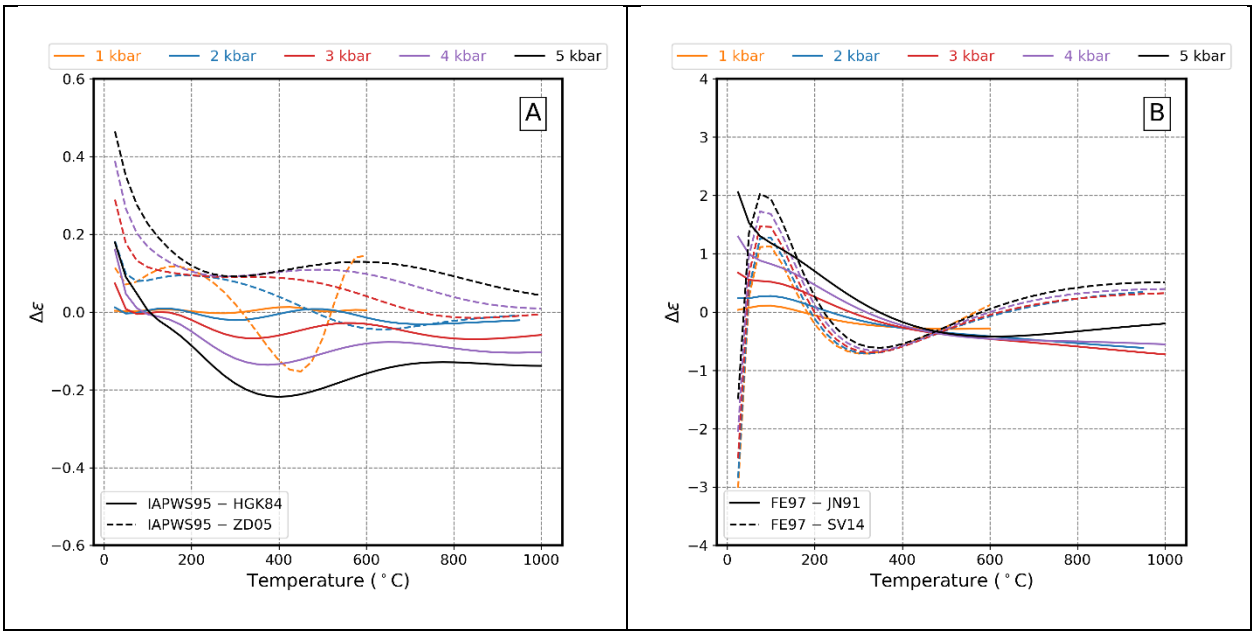

Figure S2. (A) Differences in ε_{H_2O} calculated using the FE97 model, when using the HGK84 and ZD05 models compared to the IAPWS95 model for water density.(B) Differences in ε_{H_2O}, obtained from the FE97 model, compared to the JN91 and SV14 models, all using the IAPWS95 model for water density.

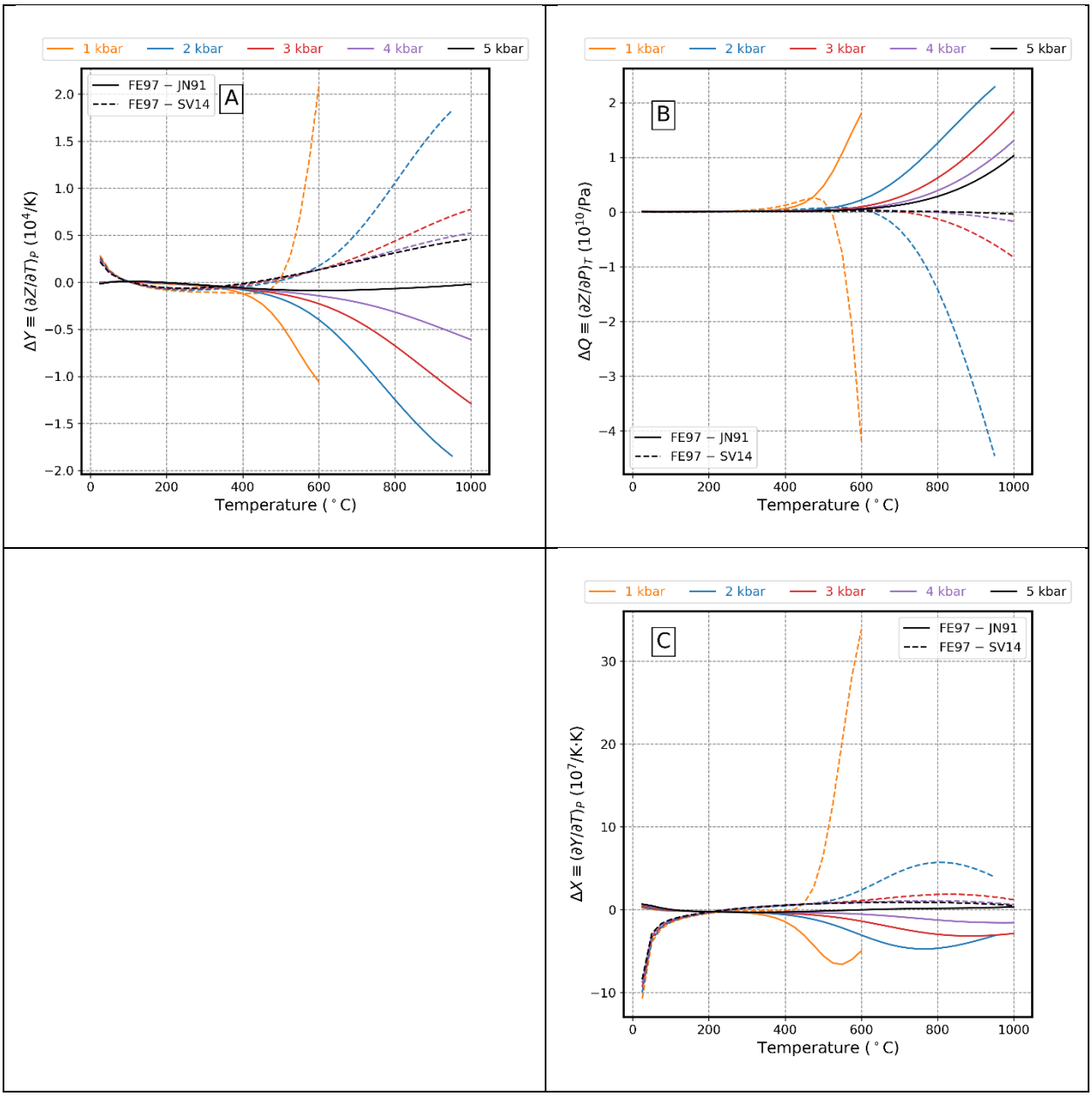

Figure S3. Differences in property values calculated with the JN91 and SV14 models for ε_{H_2O} from those obtained using the FE97 model; the IAPWS95 model is used for ρ_{H_2O} (25-1000 °C, 1-5 kbar). (A) Born Y; (B) Born Q; (C) Born X.

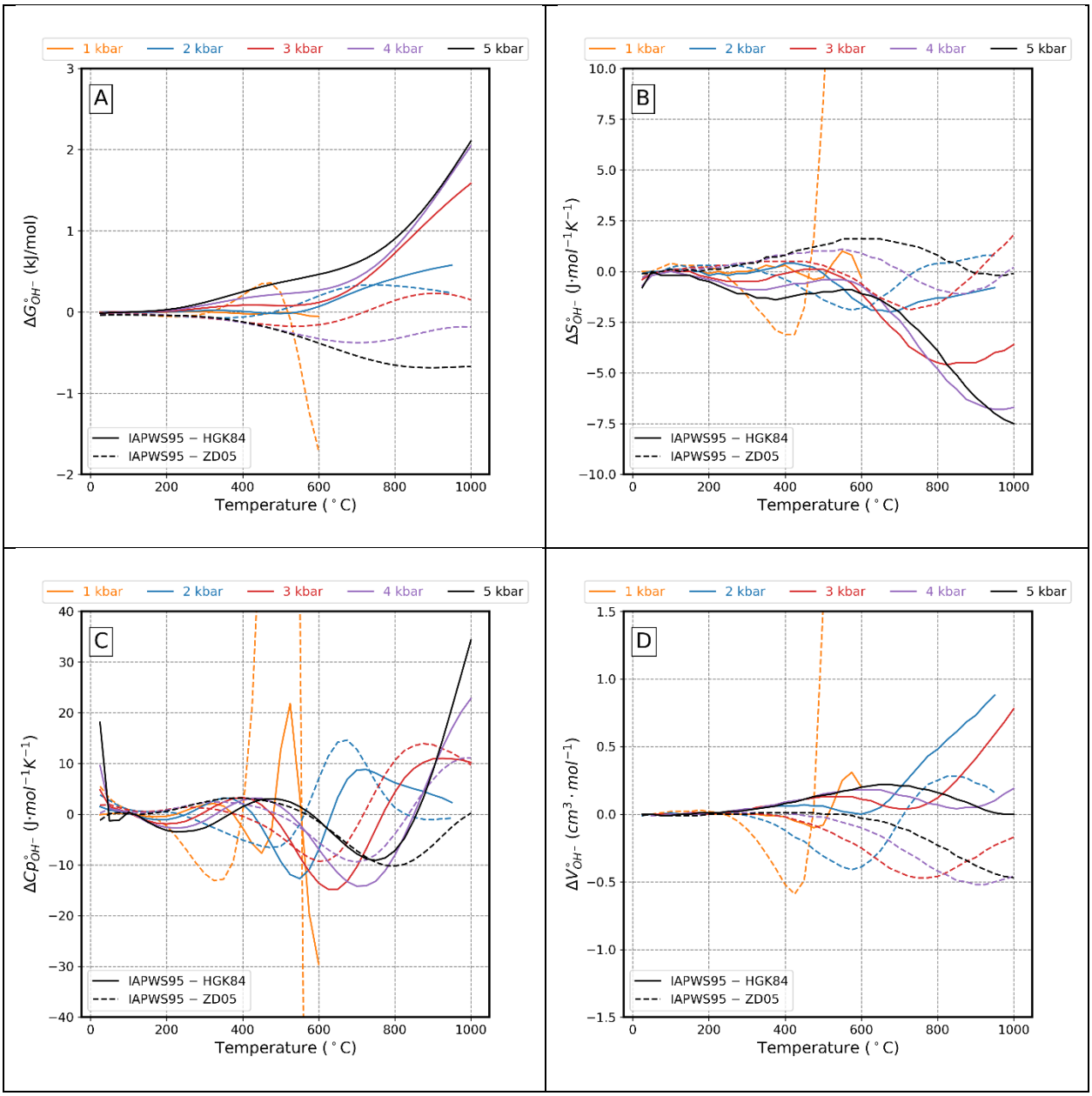

Figure S4. Differences in partial molal standard state properties of OH^-, calculated using different thermodynamic models: full line – difference between IAPWS95 and HGK84, and dashed line – between IAPWS95 and ZD05, all using the FE97 formulation for the water electrostatic properties: (A) $G^{\circ}_{\mathrm{OH^-}}$; (B) $S^{\circ}_{\mathrm{OH^-}}$; (C) $Cp^{\circ}_{\mathrm{OH^-}}$; (D) $V^{\circ}_{\mathrm{OH^-}}$.

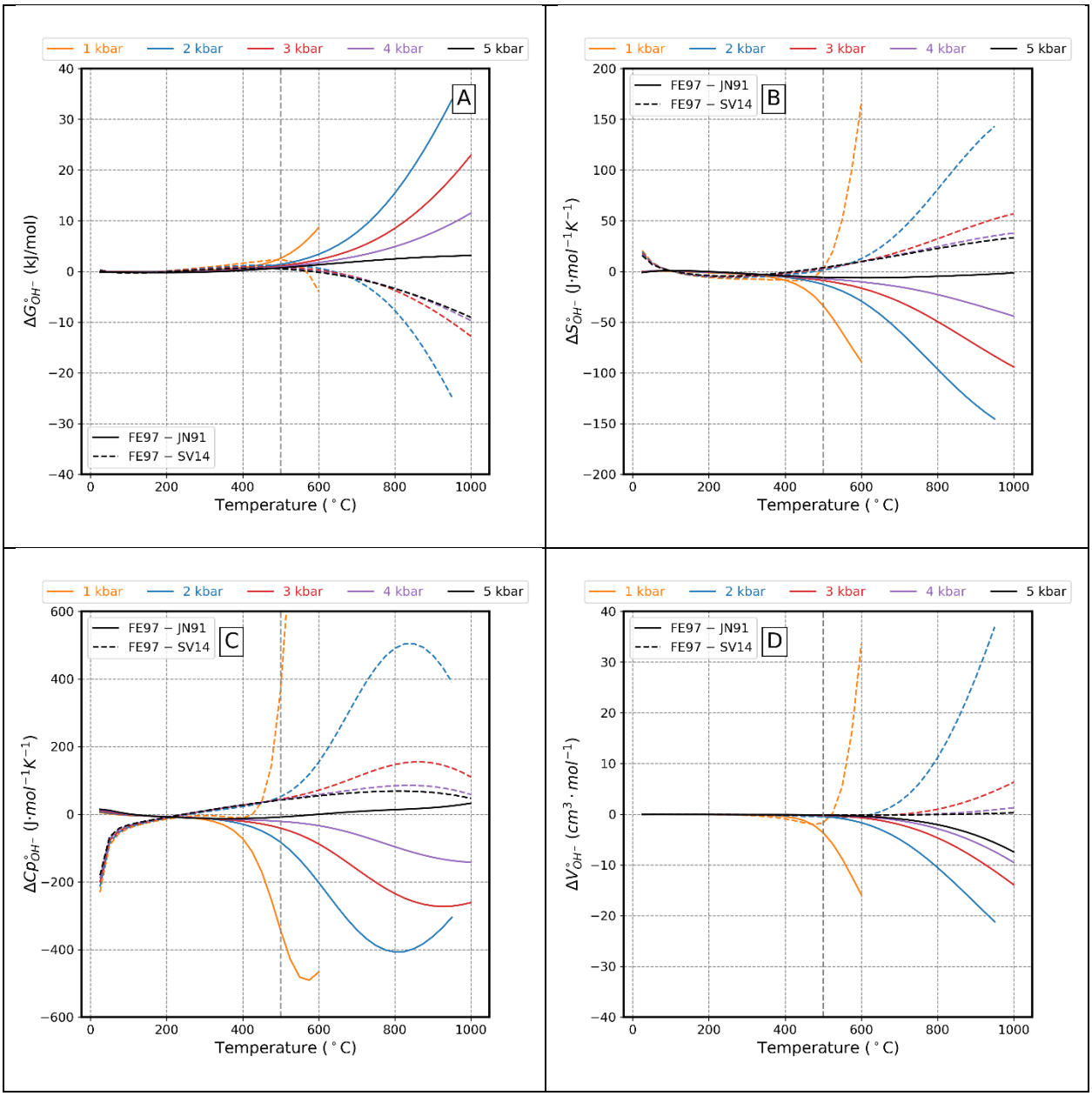

Figure S5. Differences in partial molal standard state properties of OH^-, calculated using different electrostatic models: full lines -- difference between FE97 and JN91, and dashed lines -- between FE97 and SV14 models for calculating water dielectric properties, all using IAPWS95 for water density: (A) $G^{\circ}_{\mathrm{OH^-}}$; (B) $S^{\circ}_{\mathrm{OH^-}}$; (C) $Cp^{\circ}_{\mathrm{OH^-}}$; (D) $V^{\circ}_{\mathrm{OH^-}}$. Dashed line intersects at 500 °C.